ELSEVIER

Transient apical polarization of Gliotactin and Coracle is required for parallel alignment of wing hairs in *Drosophila*

Dennis R. Venema[a,b], Tzviya Zeev-Ben-Mordehai[c], Vanessa J. Auld[a,*]

[a]*Department of Zoology, University of British Columbia, Vancouver, BC, Canada V6T 1Z4*
[b]*Faculty of Natural and Applied Sciences, Trinity Western University, Langley, BC, Canada V2Y 1Y1*
[c]*Departments of Structural Biology and Neurobiology, Weizmann Institute of Science, Rehovot, Israel*

Abstract

In *Drosophila*, wing hairs are aligned in a distally oriented, parallel array. The *frizzled* pathway determines proximal–distal cell polarity in the wing; however, in *frizzled* pathway mutants, wing hairs remain parallel. How wing hairs align has not been determined. We have demonstrated a novel role for the septate junction proteins Gliotactin (Gli) and Coracle (Cora) in this process. Prior to prehair extension, Gli and Cora were restricted to basolateral membranes. During pupal prehair development, Gli and Cora transiently formed apical ribbons oriented from the distal wing tip to the proximal hinge. These ribbons were aligned beneath prehair bases and persisted for several hours. During this time, Gli was lost entirely from the basolateral domain. A *Gliotactin* mutation altered the apical polarization Gli and Cora and induced defects in hair alignment in pupal and adult stages. Genetic and cell biological assays demonstrated that Gli and Cora function to align hairs independently of *frizzled*. Taken together, our results indicate that Gli and Cora function as the first-identified members of a long-predicted, *frizzled*-independent parallel alignment mechanism. We propose a model whereby the apical polarization of Gli and Cora functions to stabilize and align prehairs relative to anterior–posterior cell boundaries during pupal wing development.
© 2004 Elsevier Inc. All rights reserved.

Introduction

Cell polarity is a feature of epithelial sheets in *Drosophila*. Apical–basal polarity divides epithelial cells into distinct regions of apical and basolateral membranes (Peifer and Tepass, 2000; Tepass et al., 2001), while tissue polarity orientates each cell within the plane of the epithelium (Adler and Lee, 2001). Both processes require the localization of polarity determinants to precise intracellular locations (Bilder and Perrimon, 2000; Strutt, 2002). Apical/basolateral polarity is established by components of adherens and septate junctions (Bhat et al., 1999; Bilder and Perrimon, 2000; Bilder et al., 2003; Woods et al., 1996), which provide a physical connection between adjacent cells and delimit membrane domains within the cell. Tissue polarity is established by members of the *frizzled* signaling pathway through asymmetric distribution of polarity determinants at the apical cell membrane (Axelrod, 2001; Bastock et al., 2003; Strutt, 2001; Tree et al., 2002).

During pupal development, cells comprising the *Drosophila* wing epithelium extend an actin-rich prehair toward the distal tip of the wing (Wong and Adler, 1993). The resulting adult hairs are distally oriented and parallel with their neighbors; this oriented and parallel arrangement of individual hairs is an example of tissue polarity (Axelrod, 2002). Components of the *frizzled* (*fz*) signaling pathway are asymmetrically localized during pupal development and restrict prehair initiation to the distal vertex of each cell (Strutt, 2002). Loss of *fz* signaling disrupts prehair local-

* Corresponding author. Department of Zoology, University of British Columbia, 6270 University Boulevard, Vancouver, BC, Canada V6T 1Z4. Fax: +1 604 822 2416.

E-mail address: auld@zoology.ubc.ca (V.J. Auld).

ization and alters hair polarity: in *fz* mutant wings, prehairs initiate at the cell center and hair polarities may point from distal to proximal (Adler and Lee, 2001). Loss of *fz* function does not result in random hair polarities; however, in *fz* mutant wings, neighboring hairs generally retain parallel alignment to produce curved polarity vectors (Wong and Adler, 1993). The nonrandom nature of the *fz* polarity pattern indicates that an *fz*-independent mechanism functions to align hairs in parallel (Adler, 2002). No component of this system has been identified since it was first predicted by Wong and Adler in 1993 (Adler, 2002) despite the characterization of several new *fz* pathway members (Feiguin et al., 2001; Taylor et al., 1998; Usui et al., 1999; Wolff and Rubin, 1998).

The *Drosophila* septate junction is a basolateral junction between cells characterized by a ladderlike array of electron-dense material, or septa, between opposing membranes (Fristrom, 1982). The first component of the septate junction identified in *Drosophila* was Discs-large (Dlg), which was also a founding member of the PSD-95, Discs-large, and ZO-1 (PDZ) protein family (Woods and Bryant, 1991). Dlg is a cytoplasmic protein associated with SJs by an unidentified protein–protein interaction (Tepass et al., 2001), possibly through one or more of its three PDZ motifs, which are known to bind *carboxyl*-terminal epitopes of localized proteins (Songyang et al., 1997). Thus, the most likely candidate to localize Dlg to the septate junction is a transmembrane protein with a PDZ binding epitope. Additional septate junction components have since been identified: Coracle (Cor) is a cytoplasmic protein 4.1 orthologue (Fehon et al., 1994); neurexin IV is a transmembrane protein homologous to mammalian contactin-associated paranodal receptor (Caspr) (Einheber et al., 1997); and Scribble is an additional cytoplasmic PDZ domain protein (Bilder and Perrimon, 2000). Recently, the Na^+/K^+ ATPase α and β subunits (encoded by the *Atpα* and *Nrv2* loci, respectively) and Neuroglian (Nrg), a homolog of mammalian Neurofascin, were demonstrated to be localized to, and necessary for, septate junction formation (Genova and Fehon, 2003).

Gliotactin was identified as a serine esterase-like, transmembrane protein expressed on peripheral glial membranes (Auld et al., 1995). Similar to *Nrx* mutant embryos, *Gliotactin* (*Gli*) null homozygotes fail to form the glial peripheral blood–nerve barrier and are paralyzed at late embryogenesis (Auld et al., 1995). Subsequent work demonstrated that Gli is specifically localized to the tricellular subdomain of the septate junction (Schulte et al., 2003). *Gli* function is necessary for the formation of compact septae and is the first septate junction protein known that localizes specifically to the tricellular junction (Schulte et al., 2003). Due to the *Gli* lethal phase, Gli function after embryogenesis has not been studied. To further our understanding of Gli function, we have identified and characterized a series of viable *Gli* genotypes. Adult *Gli* animals had visible defects in the parallel

alignment of neighboring hairs and in adhesion at the wing margin. Examination of Gli and an additional septate junction marker, Coracle, during wing development revealed that both proteins are transiently polarized to form apical ribbons in line with hair orientation and in close juxtaposition to prehair bases. This polarization was found to be independent of the *frizzled* signaling pathway, identifying Gliotactin and Coracle as the first-known members of a predicted *frizzled*-independent parallel alignment mechanism.

Materials and methods

Fly strains and mutagenesis

Flies were grown on standard media at 22°C unless stated otherwise. The viable *Gliotactin* enhancer trap (genotype w^{1118}/Y; Gli^{AE2}/Gli^{AE2}; Auld et al., 1995) was mutagenized with EMS according to standard procedures (Ashburner, 1989) and tested for complementation against the null allele $Gli^{AE2\Delta45}$. Novel *Gli* chromosomes were serially recombined with flanking markers and retested against $Gli^{AE2\Delta45}$. Only lines that failed to complement $Gli^{AE2\Delta45}$ after recombination were retained. The *Gli* alleles $l(2)\ 35Dg^{RAR77}$ and $l(2)\ 35Dg^{P34}$ were obtained in an independent EMS screen for lethal mutations in the *snail-cactus* region (Ashburner et al., 1990) and shown to be allelic to *Gli* by complementation (Auld et al., 1995).

Sequence analysis of novel Gli alleles

For each *Gli* mutant, genomic DNA was prepared from 25 to 30 homozygous embryos as follows: 25–30 embryos were homogenized in 50 μl of homogenization buffer (10 mM Tris–HCl pH 8, 25 mM NaCl, 200 μg/ml proteinase K), incubated at 37°C for 30 min followed by 2 min at 94°C. Overlapping fragments spanning the *Gli* coding region were amplified using standard PCR conditions in 200 μM $MgCl_2$ with one unit of Taq DNA polymerase (Amersham). PCR products were gel purified (Qiaex II gel purification kit, Qiagen) and directly sequenced on both strands using an ABI PRISM automated fluorescence sequencer. Changes relative to the AE2 mutagenesis chromosome were confirmed by sequencing an independent PCR product. Primer pairs utilized were as follows: pair 1: AE2 II: 5′-CGG GAA TTC CTT TTA AAT ACA TTT CCT AC-3′ and AE2 *Hin*dII: 5′-GCC CTA GGC GAA TAC ATC CCG CTC CAG GG-3′; pair 2: AE2 III: 5′-GGA ATT CCT AAT GAT GTT ACC ATT TCC C-3′ and AE2 IV: 5′-CGG GAT CCA CCA CGT CGT AGA ACG AGG C-3′; pair 3: AE2 V: 5′-CGG GAT CCA GCC TCC AAC CTA TTC CAG GG-3′ and AE2 VI: 5′-CGG GAT CCA CGG ATG AGG GTT TCC GGC G-3′; pair 4: AE2 VII: 5′-GGA ATT CCA TTG GTA CGA GGG ATG GCG C-3′ and AE2 VIII: 5′-CCT TAA GGA GAA CTC GGT GTC CAT GAA GG-3′; pair 5: AE2

IX: 5′-GGA ATT CCA TCG AAC GTT ATT TCC TCA CCG-3′ and AE2 X: 5′-CCT TAA GGA TTA TCC CTG GAG CGC AGG GC-3′, pair 6: AE2 XI: 5′-GGA ATT CCG CGT GGA GTG GAC AAT GCC C-3′ and AE2 XIV: 5′-GCG ATC CTG CGC TTA GAG ACG-3′.

Scoring of mutant wings

Wings from relevant flies were rinsed in 95% ethanol and mounted in 85% lactic acid (BDH) or 1:1 Hoyer's mountant: 85% lactic acid and examined using bright-field microscopy while wet. Wing veins were used to divide the wing into seven major regions. The number of such regions containing a patch of nonparallel alignment was counted and averaged for 20 wings of each genotype.

Staining of pupal wings

Gli alleles were balanced over a T(2;3)SM6a-TM6B, Tb^1 balancer chromosome (Basu et al., 1999), which allowed selection of non-Tb^1, *Gli* pupae. Pupae were aged to the specified time after puparium formation at 25°C and fixed in 4% formaldehyde in PBS + 0.1% Tween 20 + 0.1% Triton X-100 for 20–30 min at room temperature. Fixed pupae were dissected in PBS + 0.1% Tween 20 + 0.1% Triton X-100 and incubated with primary antibodies for 3 h at 4°C: rabbit anti-Gliotactin polyclonal antibody (αcter) at 1:200, mouse anti-Coracle monoclonal cocktail (9C and C615 at 1:200 each; Fehon et al., 1994), and mouse anti-α spectrin at 1:10 (3A9, Developmental Hybridoma Studies Bank, University of Iowa, Iowa City, IA). Stained wings were labeled using goat anti-rabbit Alexa-488, goat anti-rabbit Cy5, and goat anti-mouse Alexa-568 secondary antibodies at 1:500 (Molecular Probes). To visualize F-actin, wings were incubated with Alexa-568 phalloidin (Molecular Probes) at 1:400. Nuclei were labeled using DAPI (Sigma) diluted to 1:200 from a 1 mg/ml stock. Wings were mounted in Vectashield (Vector Laboratories) and visualized using a Deltavision deconvolution microscope (Applied Precision). Images were deconvolved using eight iterations and assembled using Photoshop 7.0 (Adobe).

Genetic interactions

Genotypes used were as follows:

disheveled: [w^1, dsh^1/Y; b, Gli^{dv5}, cn/b, Gli^{dv5}, cn] and [b, Gli^{dv5}, dsh^+-GFP/b, Gli^{dv1}]
prickle: [b, Gli^{dv5}, cn, pk^1/b, Gli^{dv5}, cn, pk^1]

Scanning electron microscopy

Samples were sputter coated with 20 nM gold palladium using a Nanotech SEMPREP 2 and viewed at 0.8 kV with a Hitachi S4700 scanning electron microscope.

Results

Isolation and characterization of hypomorphic Gliotactin alleles

The *Gliotactin* null phenotype is paralysis and death due to an open blood–nerve barrier at the end of embryogenesis (Auld et al., 1995). No adult-viable mutant *Gli* genotypes have been reported. In order to extend our analysis of Gliotactin function postembryogenesis, we performed a mutagenesis screen and isolated a number of novel, ethyl-methane–sulfonate (EMS)-induced *Gli* alleles that failed to complement the null allele $Gli^{AE2Δ45}$. One novel allele, Gli^{dv5}, was homozygous viable (Table 1). Sequencing of this allele revealed a single, nonconservative mutation in the extracellular serine esterase-like domain (Fig. 1). Several of the novel and previously identified homozygous-lethal *Gli* alleles generated adult escapers in trans to Gli^{dv5}, resolving these alleles into an allelic series (Table 1). Structural changes underlying this allelic series were determined by sequencing each allele. Gli^{RAR77} was found to contain a nonsense mutation in the intracellular *carboxyl*-terminal region (Fig. 1). This homozygous-lethal allele generated more adult escapers in trans to Gli^{dv5} than Gli^{dv5} itself, indicating that the extracellular and intracellular domains of Gli can function together when on separate proteins (Table

Table 1
Interallelic complementation between Gli^{dv5} and homozygous-lethal *Gli* alleles reveals an allelic series based on adult escaper frequency and wing hair alignment

Cross	Escaper genotype	Gli/CyO progeny	Gli^{dv5}/Gli progeny	Frequency of escapers[a]	Wing hair phenotype[b]
Gli^+/CyO × Gli^{dv5}/CyO	Gli^{dv5}/Gli^+	782	417	1.00	0.5
Gli^{RAR77}/CyO × Gli^{dv5}/CyO	Gli^{dv5}/Gli^{RAR77}	681	291	0.80	2.9
Gli^{dv5}/CyO × Gli^{dv5}/CyO	Gli^{dv5}/Gli^{dv5}	2652	172	0.13	3.4
Gli^{dv1}/CyO × Gli^{dv5}/CyO	Gli^{dv5}/Gli^{dv1}	998	17	0.03	4.1
Gli^{dv3}/CyO × Gli^{dv5}/CyO	Gli^{dv5}/Gli^{dv3}	1100	5	<0.01	6.6[c]
Gli^{P34}/CyO × Gli^{dv5}/CyO	Gli^{dv5}/Gli^{P34}	1142	1	<0.01	ND

[a] Normalized to the Gli^{dv5}/+ genotype.
[b] The average number of wing regions containing an area with nonparallel alignment is indicated for each *Gli* genotype (n = 20 wings/genotype). ND indicates not determined.
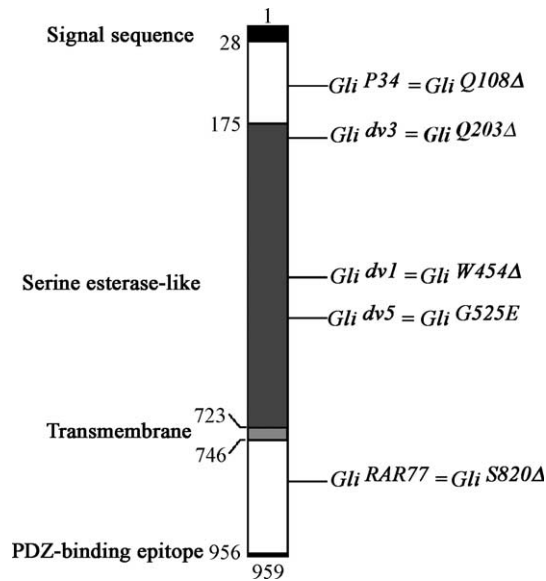[c] Indicates that wing blisters were present at the distal margin in this genotype.

Fig. 1. Domain structure of Gliotactin and location of point mutations. Gliotactin is a 959 amino-acid, type-I transmembrane protein with a signal sequence, serine esterase-like domain, and intracellular PDZ-recognition peptide. The location of several point mutations is indicated. Gli^{dv5} is a nonconservative substitution of a glutamic acid for a glycine at position 525, within the extracellular serine esterase-like domain. Gli^{P34}, Gli^{dv3}, Gli^{dv1}, and Gli^{RAR77} are nonsense mutations at positions 108, 203, 454, and 820, respectively.

1). The Gli^{dv1} allele results from a premature stop codon within the serine esterase like domain (Fig. 1); this allele escaped in trans to Gli^{dv5} at a low frequency (Table 1). Two alleles (Gli^{P34} and Gli^{dv3}) rarely escaped in trans to Gli^{dv5} (Table 1); both alleles are premature stop codons early in the Gli open reading frame (Fig. 1).

Gliotactin mutants have defects in wing hair alignment and adhesion at the wing margin

The availability of *Gli* genotypes that survive to adult stages allowed us to examine adult epithelia for mutant phenotypes. Adult wings of *Gli* mutants were examined for defects (Fig. 2). *Gli* mutants display an increasing severity of wing hair orientation defects that parallels the *Gli* allelic series (Figs. 2C–H; Table 1). The primary *Gli* wing hair phenotype was disruption of parallel alignment between neighboring hairs such that adjacent hairs converge in a chevron pattern (arrows, Fig. 2C). This phenotype was present in *Gli* wings not mounted under a coverslip (data not shown), as well as in *Gli* wings examined using scanning electron microscopy (Fig. 2M), and as such is not a mounting artifact. To quantify the *Gli* phenotype, we used veins to divide the wing into seven main regions (Fig. 2A), scored 20 wings of each genotype, and counted the number of regions that contained patches of nonparallel hairs (Table 1). The Gli^+ chromosome used for mutagenesis had the wild-type pattern of parallel, distally oriented hairs (Figs. 2B and L). In weak *Gli* genotypes, only small numbers of hairs were affected, resulting in small, infrequent mutant

patches (Fig. 2C; Table 1). Random samples of 20 Gli^{dv5}/Gli^{RAR77} or Gli^{dv5}/Gli^{dv5} wings ranged from wings with disrupted hairs in every wing region to completely wild-type wings. On average, Gli^{dv5}/Gli^{RAR77} wings had 2.9 regions with altered alignment compared to 3.4 for Gli^{dv5}/Gli^{dv5} wings. In stronger *Gli* genotypes, mutant patches were more frequent and larger (Figs. 2D and E; Table 1). All 20 Gli^{dv5}/Gli^{dv1} wings sampled had at least one region of disrupted alignment, with an average of 4.1 regions affected. In the severe Gli^{dv5}/Gli^{dv3} genotype, mutant patches covered large portions of the wing (Figs. 2F–H, J–K, and M) and were consistently present (Table 1). In a random sample of 20 Gli^{dv5}/Gli^{dv3} wings, eight had an area of disrupted alignment in six wing regions; the remaining 12 wings had disrupted alignment in all seven intervein areas, giving an average of 6.7 disrupted regions per wing. Despite this consistent phenotype, hairs with correct alignment remained in even the most severely affected Gli^{dv5}/Gli^{dv3} wings. Examples of the extent of the nonparallel phenotype in two randomly selected Gli^{dv5}/Gli^{dv3} wings are shown in Figs. 2J–K. In addition to nonparallel alignment, patches of deformed hairs were occasionally observed in all adult *Gli* genotypes, often at the anterior–posterior boundary (arrows, Fig. 2E). Deformed hairs were thinner than normal and were often bent. A third phenotype, blistering at the distal margin, was observed in the strongest *Gli* genotype, Gli^{dv5}/Gli^{dv3} (dashed outline, Fig. 2H; Table 1). In a sample of 20 Gli^{dv5}/Gli^{dv3} wings, 7 contained blisters. Such blisters were always in contact with the distal margin.

To examine if hair alignment and blistering phenotypes were unique to *Gli* or present in additional septate junction mutants, we examined adult wings mutant for *coracle*. In the $coracle^5$/$coracle^{15}$ genotype, wing hairs are misaligned in a manner indistinguishable from the *Gli* pattern (Fig. 2I). We did not observe blistering in this genotype.

We reasoned that the observed *Gli* wing phenotypes may result from either a partial reduction or the complete loss of Gli function in the wing. To resolve this question, we recombined the Gli^{dv3} allele onto an FRT chromosome and induced somatic recombination with the heat shock-Flp recombinase system (Xu and Rubin, 1993) to generate Gli^{dv3}/Gli^{dv3} cells in a Gli^{dv3}/+ heterozygous wing. We were unable to obtain adult clones homozygous for Gli^{dv3}, indicating that Gli is required for cell survival. As a control, we successfully identified transient Gli^{dv3} clones in pupal wings by pairing the FRT Gli^{dv3} chromosome with an FRT chromosome expressing ubiquitin-GFP. Such clones were short lived and eliminated before the onset of prehair extension (data not shown). As an additional control, we examined Gli^{dv5} clones in adult wings. Such clones exhibited a phenotype equivalent to homozygous Gli^{dv5} wings (data not shown). These results indicate that wing cells require Gli function to survive and that the observed *Gli* phenotypes result from partial, not complete, loss of Gli function in wing cells.
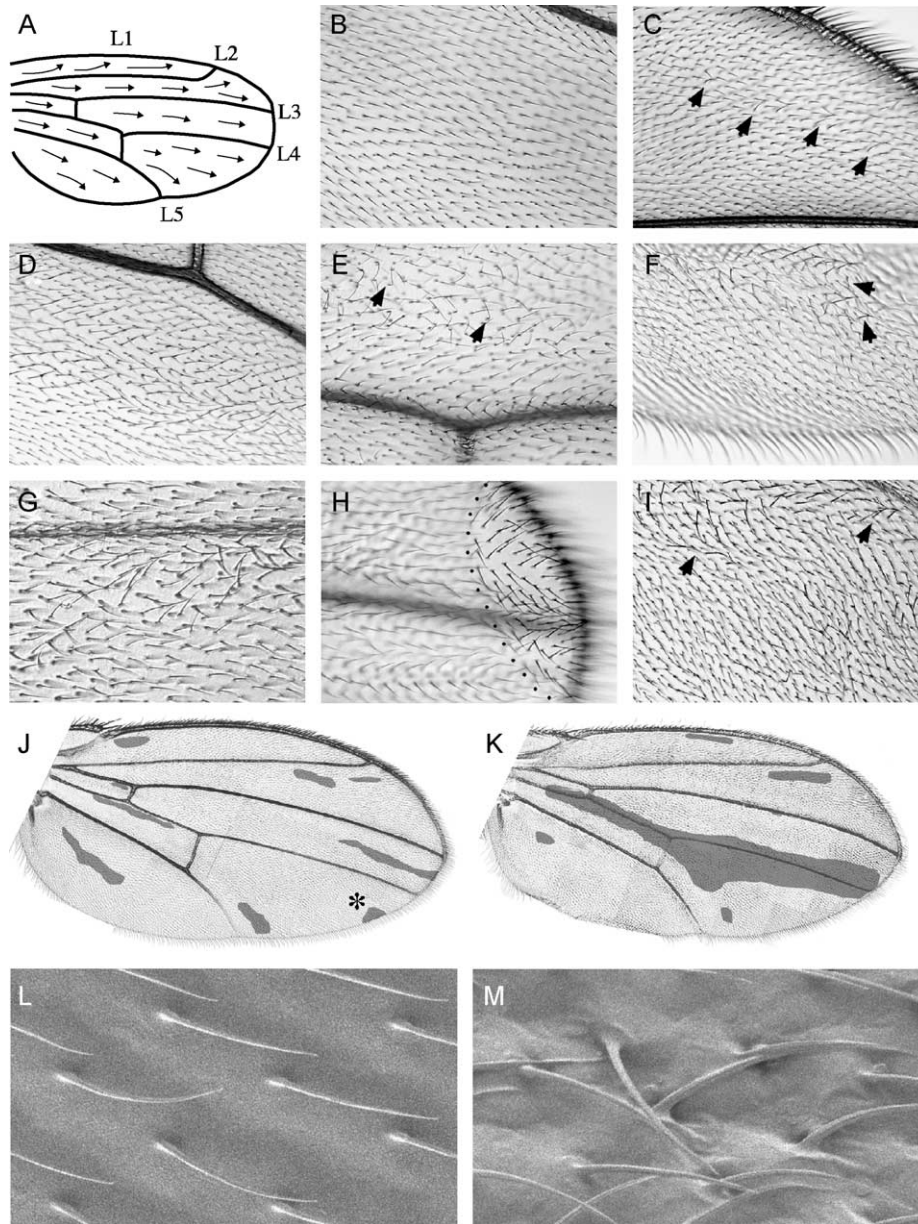
Fig. 2. *Gli* mutants have defects in parallel alignment and adhesion at the wing margin. Veins divide the wing into seven major regions (A). Arrows indicate the orientation of hairs. Hairs are aligned in parallel and point distally in the *Gli*+ chromosome used for mutagenesis (B). (C) is an example of the *Gli*dv5/*Gli*RAR77 phenotype. Several hair "chevrons" (arrowheads) are visible on an otherwise normal wing. (D) Region posterior to the posterior cross vein on a *Gli*dv5/*Gli*dv5 wing. Numerous hairs have disrupted alignment and form a continuous patch across this area. (E) Example of the deformed hair phenotype observed occasionally in all *Gli* genotypes (*Gli*dv5/*Gli*dv1 wing shown). Numerous hairs are bent and abnormally thin (arrows). Examples of the *Gli*dv5/*Gli*dv3 phenotype are shown in (F–H). Chevrons are indicated with arrows in (F); a distal blister is outlined in (H). In *Gli*dv5/*Gli*dv3 wings, large regions have multiple patches with nonparallel alignment (F). Foci of nonparallel hairs with normal neighbors are also seen in this genotype (G), as well as blisters on the distal margin (H). Nonparallel hairs are also present in *cora*5/*cora*15 mutants (I); arrows indicate chevrons. Regions of nonparallel alignment are shaded in two example *Gli*dv5/*Gli*dv3 wings (J and K), showing the variability in the extent and size of mutant patches in this genotype. An asterisk indicates a marginal blister in J. Large regions of properly aligned hairs remain even in severely affected *Gli*dv5/*Gli*dv3 wings (K). (L and M) Scanning electron micrographs of wild-type and *Gli*dv5/*Gli*dv3 wing hairs, respectively. The wing cuticle remains flat in regions of disrupted hair alignment (M), although it appears rougher than wild type (L).

Gliotactin and Coracle are transiently polarized during wing development

Gliotactin is localized to the tricellular septate junction in the embryonic epidermis and is required for the formation of mature septa (Schulte et al., 2003). In the absence of Gli function, additional septate junction components such as Cora, Dlg, and Nrx are mislocalized (Schulte et al., 2003). We assayed Gli and Cora expression in pupal wings using immunofluorescence. At 30 h after puparium formation (APF), Gli is localized to the tricellular septate junction in the developing wing, where it overlaps with Coracle (Fig. 3A–C). This pattern of Gli and Cora staining is identical to that found in the embryonic epidermis (Schulte et al., 2003).
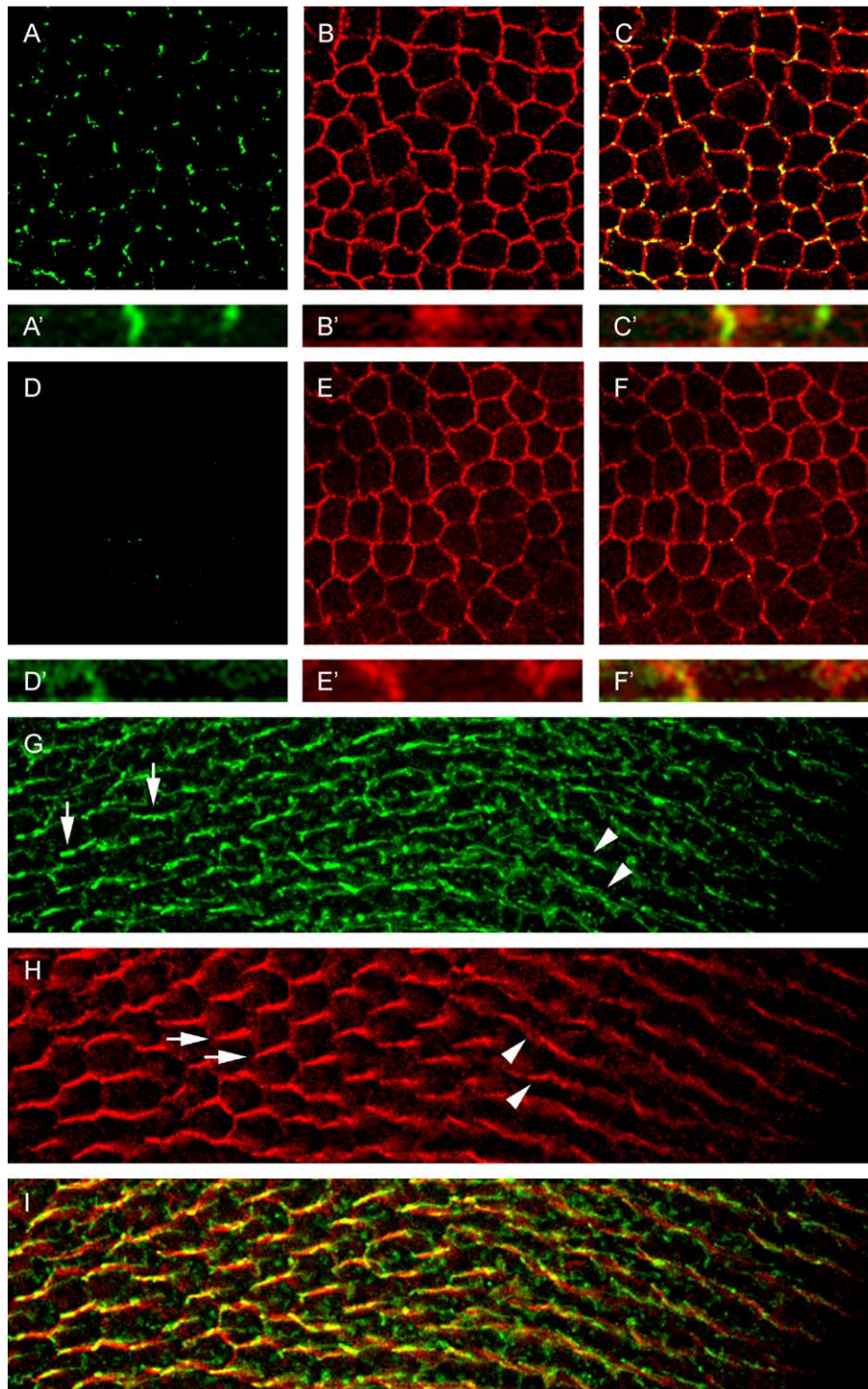
Fig. 3. Gli and Cora localization in the pupal wing from 30 to 35 h APF. The location of Gli (green) and Cora (red) in pupal wings at 30 h, APF was determined using immunofluorescence. In wild-type wings (A–C′), Gli is present at tricellular corners (A), while Cora is present around the cell circumference (B). Cora and Gli colocalize at the tricellular septate junction (C). In the apical–basal plane, Gli (A′) and Cora staining (B′) share the same domain, overlapping at basolateral tricellular junctions (C′). In homozygous Gli^{dv5} wings (D–F), only small amounts of Gli immunoreactivity were present at tricellular corners (D and D′). Cora staining was unaffected (E and E′). The Gli staining present in this genotype colocalized with Cora at the level of the septate junction (F and F′). At 35 h APF, both Gli and Cora were remodeled into apical ribbons beginning at the wing margin (G–I). The wing margin is to the right. Gli localization spread from tricellular corners to label anterior posterior boundaries (G, arrows), while Cora became diffuse on proximal–distal boundaries that remained staggered (H, arrows). Subsequently, polarized Gli and Cora were aligned into continuous ribbons (G and H arrowheads). This process progressed from the wing margin inwards.

We assayed Gli and Cora localization in Gli^{dv5}/Gli^{dv5} and Gli^{dv5}/Gli^{dv3} pupal wings at 30 h APF to assess the effect of partial Gli loss-of-function on the localization of these two proteins. Gli immunofluorescence at the tricellular junction was severely reduced in the Gli^{dv5}/Gli^{dv5} genotype (Figs. 3D–F') and not detectable in Gli^{dv5}/Gli^{dv3} wings (data not shown); Cora was correctly localized in both mutant Gli genotypes.

Gli and Cora localization remained stable until approximately 35 h APF, when a rearrangement of both proteins was observed beginning at the wing margins (Figs. 3G–I). Cora staining became diffuse in the anterior–posterior axis while remaining sharp in the proximal–distal axis to form a ribbon oriented from the distal margin towards the wing hinge (Fig. 3H). Similarly, Gli was lost from the tricellular junction and was reordered into distal-to-proximal ribbons partially overlapping with Cora staining (Figs. 3I and H). This dramatic reorganization of Cora and Gli occurred within the apical–basal dimension as well. At 30 h APF, Gli at tricellular junctions colocalizes with α-spectrin (Figs. 4A–C), with extensive overlap in the apical–basal plane (Figs. 4A'–C'). The region of Gli/spectrin overlap is at the level of nuclei visualized with DAPI staining (Figs. 4A and A'). At 38 h APF, Gli staining extended apically to abut prehair bases labeled with phalloidin (Figs. 4D–F') and was present only in the apical domain of α-spectrin staining (Fig. 4D'). The apical ribbons of Gli were often aligned beneath prehair bases but did not overlap with them (arrowheads, Fig. 4F', cross section is perpendicular to the Gli ribbons). Junctional Gli staining at 30 h APF is restricted to the basolateral cell boundary (Figs. 4A–C), but apical Gli ribbons only partially overlap junctional F-actin at 38 h APF (inset, Figs. 4D–F). The hexagonal packing of cells in the wing aligns a given prehair base at the cell center with the anterior/posterior cell boundaries of the cells proximal and distal to it. Gli ribbons ran parallel to cell boundaries and also traversed cells from distal to proximal vertices to pass near the centrally located prehair base, running from prehair to prehair in line with the interposed anterior–posterior cell margin (arrowheads, Figs. 4D–F, inset).

In addition to Gli, Cora staining at 38 h APF was also apically extended (Figs. 4G–I'). Cora was present as distal–proximal ribbons just basal to prehair bases (Figs. 4G–I). In cross section, Cora staining was present apical to nuclei (arrowheads, Fig. 4G', cross section is perpendicular to the Cora ribbons) and approached prehair bases (arrowheads, Fig. 4I'). In contrast to Gli, Cora staining at 38 h APF persisted in the basolateral domain, where it remained around the entire cell cortex (Figs. 4G'–I''). Cortical Cora staining was visible in sections at the level of nuclei (Fig. 4G'') where it overlapped small amounts of junctional F-actin (Fig. 4H'').

Apical reorganization of Gli and Cora progressed across the wing from the margins inwards and was complete by approximately 37 h APF (Figs. 5A–C''). Double labeling for Gli and Cora at this time point revealed that apical ribbons of each protein did not precisely colocalize. Close association and partial overlap of the two is evident in both en face views (Fig. 5C) and in cross sections (Figs. 5C' and C''); however, Gli staining was present apical to the Cora ribbon. Gli extension apical to Cora is visible in cross sections perpendicular to the ribbon axis (arrowheads, Fig. 5C') and aligned with the ribbon (arrowheads, Fig. 5C''). This finding was in agreement with the closer association of Gli to prehair bases than Cora (compare Figs. 4F' and I').

The apical rearrangement of Gli and Cora took place in Gli^{dv5}/Gli^{dv5} wings; however, Gli staining was reduced in this genotype and was more punctate in nature (Figs. 5D and F). Additionally, Cora recruitment to apical ribbons was less sharp in Gli^{dv5}/Gli^{dv5} wings than in wild type (Figs. 5E and F; compare to Figs. 5B and C), a finding in contrast to the wild-type Cora pattern observed previously at 30 h APF. At 40 h APF, apical Gli and Cora remain in ribbons in wild-type wings (Figs. 5G–F); however, in the Gli^{dv5}/Gli^{dv5} genotype, Gli staining is absent and Cora is diffuse (Figs. 5J–L).

We extended our analysis of Gli and Cora localization to 47 h APF. Apical ribbons of Gli and Cora were absent in wild-type wings at this stage (data not shown). In the basolateral domain, Cora localization was sharp around the cell cortex (Fig. 6B). Gli staining in the basolateral domain was weak and diffuse around the cell with small concentrations at tricellular corners (Fig. 6A). This reestablishment of a 30-h APF-like Cora pattern occurred in Gli^{dv5}/Gli^{dv5} tissue; however, Cora localization was less sharply defined in this genotype (Fig. 6E). Gli staining at 47 h APF was not detectable in Gli^{dv5}/Gli^{dv5} wings (Fig. 6D).

The Gli nonparallel phenotype arises after prehair extension

To assess the effect of Gli mutations on prehair initiation, we stained Gli mutant wings using Alexa-568 phalloidin. In wild-type wing epithelia 32 h after puparium formation (APF), a ring of junctional actin was present around the cell periphery and prehairs were visible emerging from the distal vertex of each cell (Fig. 7A). In the Gli^{dv5}/Gli^{dv3} genotype, junctional and prehair F-actins were present and prehairs initiated correctly at the distal vertex (Fig. 7B). At 38 h APF, prehairs have extended further and are aligned in parallel in wild-type wings (Fig. 7C). Interestingly, alignment at 38 h APF is normal in Gli^{dv5}/Gli^{dv3} wings (Fig. 7D). Between 38 and 45 h APF, prehairs were too flexible to give an accurate indication of alignment. Starting at about 45 h APF, prehairs became more rigid and the prehair pedestal labeled with phalloidin. The pedestal remained visible until about 47.5 h APF when phalloidin staining became impractical due to deposition of the pupal cuticle. At 47 h APF in wild-type wings, prehair pedestals lie flat within the plane of the epithelium and present a circular cross section in an en face view (Fig. 7E). In Gli mutant wings, prehair pedestals were occasionally
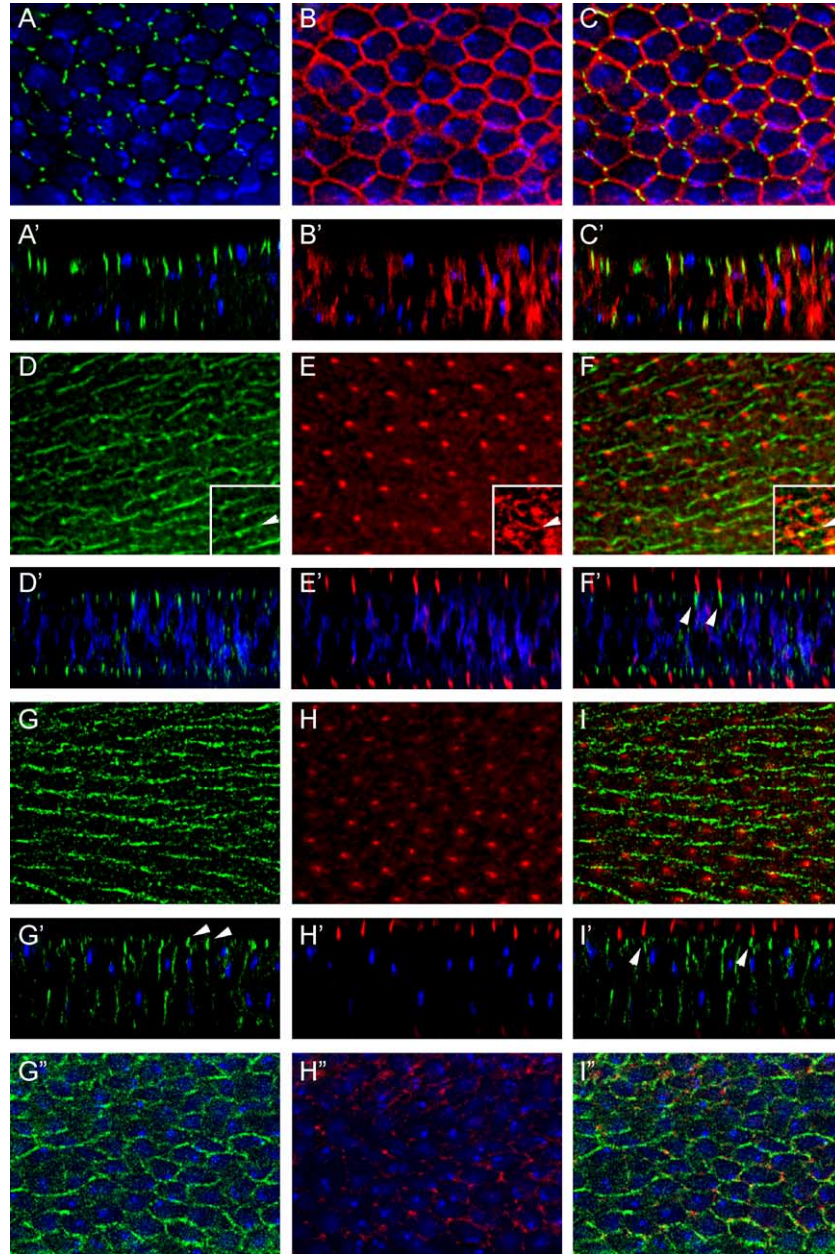
Fig. 4. Gli and Cora ribbons align with prehair bases at 38 h APF. (A) Gli (green) is tricellular at 30 h APF. Nuclei are labeled in blue. In cross section, Gli is present at the level of nuclei (A′). The α-spectrin (red) labels cell cortices in en face (B) and cross-section views (B′). There is substantial overlap between Gli and α-spectrin at tricellular junctions (C and C′). At 38 h APF, Gli (green in D and D′) is apically restricted and close to prehair bases labeled with phalloidin (red in E and E′). The merged en face view is shown in F, the merged cross section (F′) includes α-spectrin staining (blue). The cross section is perpendicular to the Gli ribbons. Arrowheads indicate close juxtaposition of Gli ribbons and prehair bases. Overexposure for F-actin staining reveals the alignment of the Gli ribbon with prehair bases and anterior–posterior cell boundaries labeled with phalloidin (arrowhead, D–F inset). Cora (green) relative to F-actin (red) and nuclei (blue) at 38 h APF is shown in G–I″. Apical Cora (G) is present in ribbons close to prehair bases (H). Panel I gives the merged image. In a cross section perpendicular to the apical Cora ribbons (G′–I′), Cora ribbons are apical to nuclei (arrowheads, G′). Prehairs labeled with phalloidin (H′) are aligned with Cora ribbons (arrowheads, I′). In the basolateral domain at 38 h APF, Cora remains around the cell cortex (G″) along with small amounts of junctional F-actin (H″). Panel I″ gives the merged image.

tilted within the epithelial plane and were narrower than normal in cross section (arrows, Fig. 7F). We did not quantify this phenotype in the same manner as the adult wing since only a small portion of the pupal wing is accessible for study at 47 h APF due to extensive folding, and the prehair pedestal does not label with phalloidin later in development. The pedestal phenotype appears to be the pupal equivalent of the adult hair phenotype (compare with Fig. 2M); however, the frequency of tilted pedestals observed at 47 h APF was less than the frequency of nonparallel hairs in the adult. Despite these caveats, we did not observe a tilted pedestal phenotype in wild-type wings.
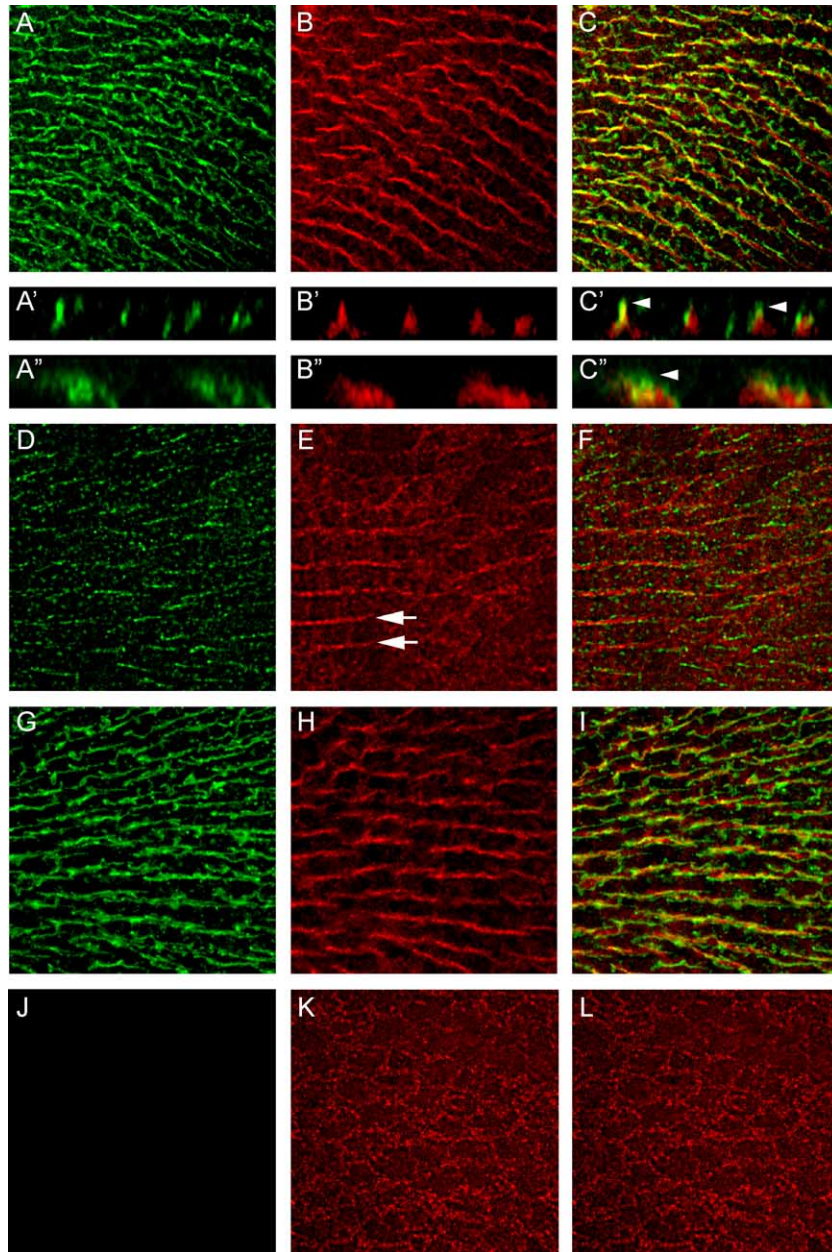
Fig. 5. Gli and Cora localization in the pupal wing from 37 to 40 h APF. By 37 h APF, Gli (A) and Cora (B) are polarized to apical ribbons over much of the wing (merge shown in C). In cross section, Gli (A and A″) is partially apical to Cora (B′ and B″). Merged images of a section perpendicular (C′ and parallel (C″) to the ribbon are shown. Arrowheads indicate Gli apical to Cora. In homozygous Gli^{dv5} wings at 37 h APF, Gli polarization is compromised (D). Apical Gli staining in this genotype was weaker than in wild-type wings, as well as more punctate in nature (compare to A). Apical Cora polarization is also affected in this genotype (E). While some polarization was evident (E, arrows), large areas without sharp polarization were present. The merged image is shown in F. In wild-type wings at 40 h APF, apical Gli remained polarized in continuous ribbons (G) where Cora was also present (H). The merged image is shown in I. In contrast to wild-type, Gli is not detectable in homozygous Gli^{dv5} wings at 40 h APF (J), and apical Cora is diffuse and nonpolar. The merged image is shown in L.

It thus appears that while the *Gli* phenotype is first visible at 47 h APF, more prehairs become unstable later in development.

Gli and Cora are independent of the frizzled pathway

Several observations suggested that septate junction-mediated parallel alignment functions independently of the *frizzled* pathway. Disruption of the adult wing hair pattern in *Gli* mutants differed markedly from *frizzled* pathway mutants. The primary *Gli* phenotype is nonparallel alignment of neighboring hairs with overall proximal–distal polarity, whereas *fz* pathway mutants largely retain parallel alignment but are incorrectly polarized. Secondly, all *fz* pathway mutants produce at least a low frequency of multiple hairs per cell, a phenotype not observed in *Gli*
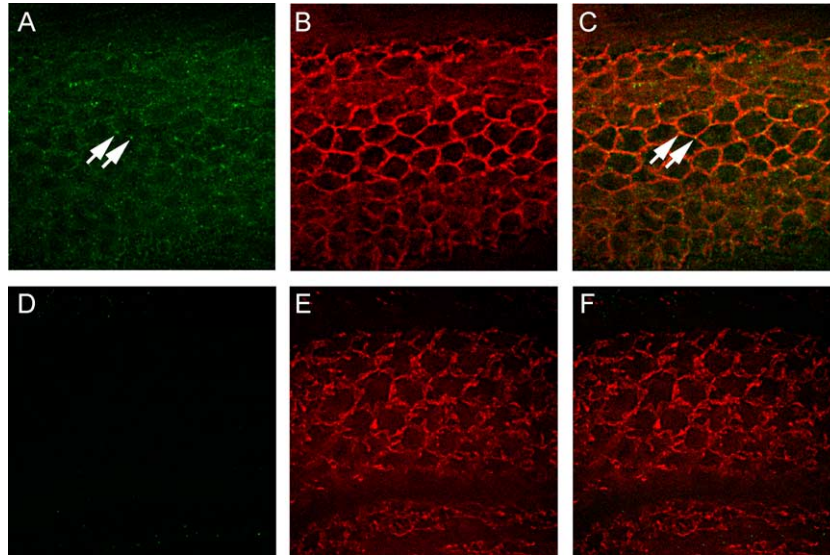
Fig. 6. Gli and Cora localization in the pupal wing at 47 h APF. In wild-type wings at 47 h APF, apical Gli and Cora are absent (not shown). Basolateral Gli staining was weak and diffuse around the cell cortex (A) with only slight concentrations at tricellular junctions (arrows, A and C). Basolateral Cora remained sharp around entire cell boundaries (B). The merged image is shown in C. In homozygous Gli^{dv5} wings at 47 h APF, basolateral Gli remained undetectable (D). Basolateral Cora was cortical in this genotype but not as sharply defined as in wild type (E). The merged image is shown in F.

wings, nor in *Gli* wings enhanced by additional septate junction mutations. Thirdly, prehairs initiate correctly at the distal vertex in *Gli* mutants, in contrast to the cell center or nondistal periphery in *fz* pathway mutants. Fourthly, apical Gli/Cora polarization occurs long after the end of *fz* signaling. Fifthly, the axis of Gli/Cora ribbons is perpendicular to the axis of polarized *fz* pathway members. Lastly, the *Gli* phenotype does not arise until long after prehair initiation, when the *fz* mutant phenotype is already evident. Given these differences between the *Gli* and *fz* wing phenotypes, we suspected that *Gli* acted independently of *fz*. We tested this hypothesis in three ways: by examining Gli and Cora localization and polarization in the absence of *fz* signaling; by assaying Disheveled (Dsh) polarization in a *Gli* mutant background; and by performing epistasis analysis in wings simultaneously mutant for *fz* signaling and *Gli*.

The dsh^1 allele produces a protein product that fails to polarize to the distal side of cells, blocking the function of the *fz* signaling pathway (Axelrod, 2001; Axelrod et al., 1998). In a homozygous dsh^1 wing, Gli was correctly localized to the tricellular septate junction at 30 h APF (Figs. 8A–C). Similarly, apical Gli and Cora were polarized correctly at 37 h APF in the dsh^1 genotype (Figs. 8D–F), demonstrating that polarization of these proteins is independent of *fz* signaling. Conversely, a functional Dsh construct tagged with green fluorescence protein (Dsh-GFP) (Axelrod, 2001) was correctly polarized in a *Gli* mutant background at 30 h APF (Fig. 8G). Epistasis analyses between *fz* pathway members and *Gli* were consistent with these results. Flies hemizygous for dsh^1 and homozygous for Gli^{dv5} exhibited the *Gli* nonparallel phenotype superimposed on the *dsh* mutant pattern (Figs.

8H and I). Similarly, flies simultaneously homozygous for *prickle* (pk^1) and Gli^{dv5} have both phenotypes (Figs. 8J and K). We assayed the location of prehair initiation in the Gli^{dv5}, pk^1 double mutant using Alexa 568-phalloidin to label F-actin (Fig. 8I). Prehair initiation occurred in the *pk* position at the cell center in the double mutants. This indicates that the *Gli* nonparallel phenotype is independent of the site of prehair initiation. Taken together, these results demonstrate that the function of Gli and Cora in parallel alignment is independent of *fz* signaling.

Discussion

Gliotactin and Coracle are transiently polarized during prehair extension

In *Drosophila*, septate junctions are initially formed during embryogenesis: these septate junctions persist in epithelia derived from the epidermis, such as imaginal structures (Tepass et al., 2001). In all previously examined tissues, septate junctions, once formed, appear static in the absence of cell division. In contrast, Gli and Cora are extensively remodeled during wing development at several time points in postmitotic cells. The initial Gli/Cora pattern in the wing before prehair extension is identical to that of the embryonic epidermis (Schulte et al., 2003). Indeed, Gli and Cora remain stable until after prehair extension at approximately 32 h APF. Beginning at 35 h APF, Gli and Cora are apically polarized at the wing margins. The initial stages of Cora polarization have been noted previously (Eaton et al., 1996); however, this previous study did not assay Cora localization past 35 h APF or examine mutant
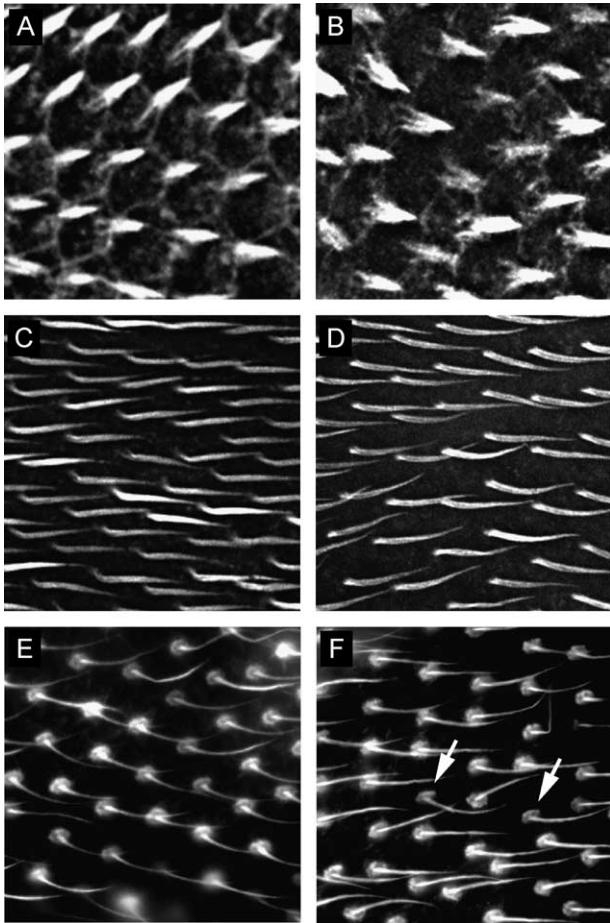
Fig. 7. The *Gli* wing hair phenotype arises after prehair elongation. Wild-type (A, C, and E) and mutant *Gli* (B, D, and F) pupal wings were stained with phalloidin to label F-actin at 32 h APF (A–B), 38 h APF (D–C), and 47 h APF (E–F). In wild-type wings at 32 h APF, prehairs were visible emerging from the distal vertices of cells (A). In *Gli^dv5*/*Gli^dv3* wings, prehairs emerged correctly at the distal vertex (B). At 38 h APF, prehairs were aligned in both wild-type (C) and *Gli^dv5*/*Gli^dv3* wings (D). At 47 h APF in wild-type wings, prehair pedestals are visible and lie flat within the plane of the epithelium (E). In homozygous *Gli^dv5* wings, pedestals were present, which were tilted within the epithelial plane (arrows, F).

cora genotypes. By 37 h APF, Gli and Cora were colocalized to continuous apical ribbons across the pupal wing. These ribbons ran along anterior–posterior cell boundaries and between proximal and distal vertices, passing just basal to prehair bases. At this stage, Gli was absent from basolateral membranes, yet Cora retained its basolateral pattern. This pattern remained stable until at least 40 h APF. By 47 h APF, Cora had lost its apical polarization and was present only around the basolateral cell periphery. In contrast, Gli was lost apically and basolaterally with only minimal Gli present on basolateral membranes, which was not predominantly tricellular at 47 h APF. It may be that the weak tricellular staining of Gli at this time point represented the start of relocalizing Gli to the tricellular septate junction; examination of Gli at stages after 47 h APF is underway to test this possibility.

The dynamic rearrangement of these junction components is, to our knowledge, without precedent in the literature. While septate junction components such as Discs-large, Coracle, Neurexin IV, Neuroglian, and the Na$^+$/K$^+$ ATPase are expressed in wing discs (Baumgartner et al., 1996; Genova and Fehon, 2003; Lamb et al., 1998; Woods and Bryant, 1991), these studies have not examined the localization of septate junction components past 30 h APF nor examined mutant genotypes for wing hair or adhesion phenotypes. Thus, it is an open question whether these septate junction proteins also are dynamic during later stages of wing development. It remains to be seen whether these components are recruited to the apical Gli/Cora ribbon and if their basolateral localization at septate junctions is modified during Gli and Cora polarization.

Loss of Dlg function in wing discs causes an overgrowth phenotype (Woods and Bryant, 1991) that includes loss of apical–basal polarity (Woods et al., 1996). In contrast to Dlg, *cora* null clones do not survive to adult stages (Lamb et al., 1998). Additionally, clones for null alleles of *Nrg* and *Nrv2* do not survive (Genova and Fehon, 2003), consistent with our results that null *Gli* clones are cell lethal. Given the essential nature of the septate junction for both proliferation control and cell viability, it will not be possible to assess the adult wing phenotype for complete loss of septate–junction function. Attempts to induce null *Gli* clones after 30 h APF have not proved successful since cell division in the wing ceases around this stage. Null clones induced during the last round of cell division did not survive long enough to examine the start of Gli/Cora polarization at 35 h APF.

Gli and Cora are required for parallel hair alignment

The polarization of Gli and Cora to apical ribbons is compromised in *Gli* mutant wings, which in turn leads to unstable prehairs later in development. The close proximity of the Gli ribbon to the prehair base, and the orientation of the ribbon along the axis the hairs will align to, is compelling evidence for a physical connection between prehairs and Gli/Cora ribbons that is required for hair alignment. In *Gli* mutant wings, the polarization of apical Gli and Cora is incomplete; additionally, it does not persist for the correct length of time. In wild-type wings, Gli and Cora remain polarized until at least 40 h APF; in contrast, in *Gli* mutant wings Gli is lost altogether by 40 h APF and Cora is no longer polarized. Thus, the *Gli* nonparallel phenotype seems to result from either a lack of apically polarized Gli/Cora or an insufficient time span of their polarization, or perhaps a combination of both. In either case, the nonparallel phenotype seems to arise from a failure to properly polarize apical Gli and Cora, which in turn leads to prehair instability later in development.

Though apical Gli and Cora define the distal-to-proximal axis in the wing, how they are connected to the prehair for its stabilization remains unresolved. The separation between the prehair base and the apical ribbon of Gli and Cora
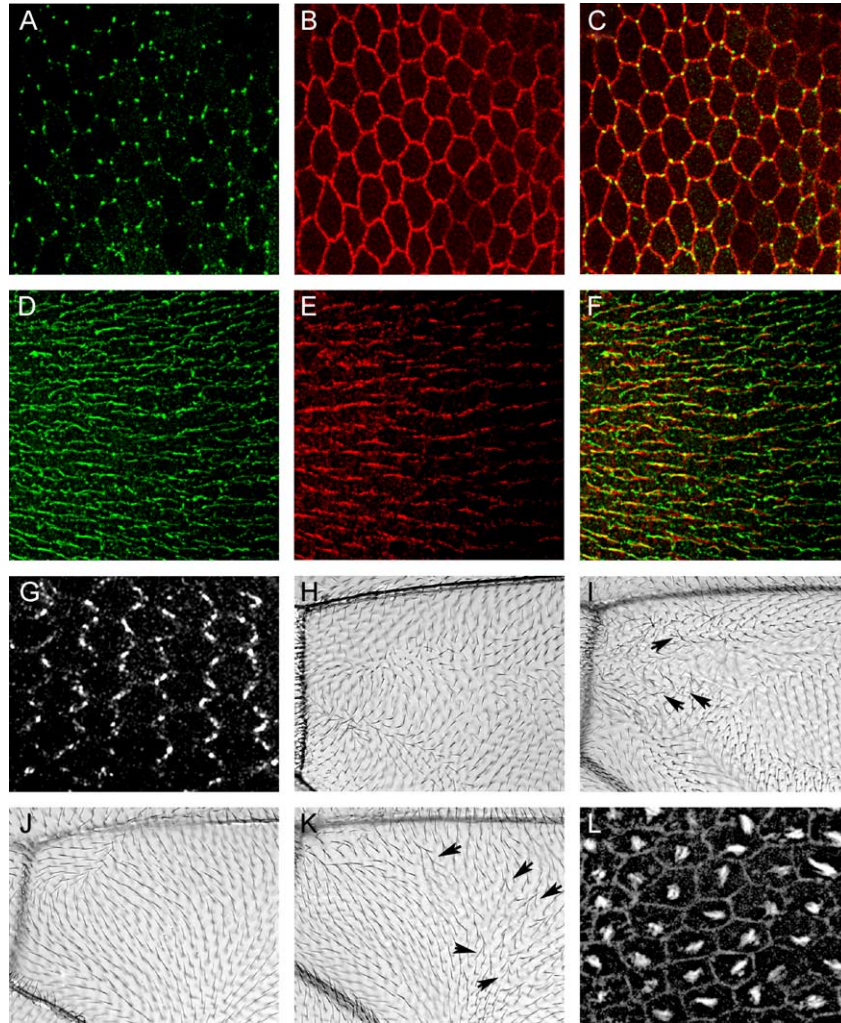
Fig. 8. Gli and Cora are independent of *frizzled* signaling. Gli immunoreactivity (green) was present at tricellular corners in *dsh¹* mutant wings at 30 h APF (A). Cora staining (red) was also normal (B), and the two septate junction markers colocalize appropriately at tricellular corners (C). At 37 h APF, apical Gli was correctly organized in the *dsh¹* mutant (D), as was Cora (E). The merged image is shown in F. The location of a functional Dsh protein tagged with GFP was assayed in *Gli^dv5^/Gli^dv1^* wings at 30 h APF (G). The distal accumulation of the Dsh-GFP transgene was unaffected in this genotype. (H) The *dsh¹* adult wing with characteristic polarity defects. The same region in a *dsh¹; Gli^dv5^/Gli^dv5^* wing is shown in I. The overall *dsh* mutant pattern is preserved, and the *Gli* nonparallel phenotype is superimposed on it (arrows). An equivalent result was obtained using a *Gli:pk* double mutant. The *pk¹* pattern is shown in J; the equivalent region of a *Gli^dv5^, pk¹/Gli^dv5^, pk¹* wing is shown in K. In the double mutant, both the *pk* and *Gli* phenotypes are present. Arrows indicate examples of nonparallel hairs. Prehair location in a *Gli^dv5^, pk¹/Gli^dv5^, pk¹* pupal wing at 32 h APF is shown in L. Prehairs were present at the cell center in the double mutant.

passing beneath it suggests an intermediate link between the two structures. A possible candidate to connect the Gli/Cora ribbon to the prehair pedestal is the cytoskeleton. Physical and genetic links between septate junction components and the cytoskeleton have previously been reported. Both subunits of the Na$^+$/K$^+$ ATPase are localized to the septate junction and physically interact with ankyrin (Nelson and Veshnock, 1987), which acts as an adapter between transmembrane proteins and the spectrin/F-actin network (Bennett and Gilligan, 1993). In *Drosophila*, the subcellular location of the Na$^+$/K$^+$ ATPase is disrupted in β spectrin mutants (Dubreuil et al., 2000). Additionally, Neuroglian clustering assembles ankyrin at cell–cell contacts through physical association (Dubreuil et al., 1997; Jefford and Dubreuil, 2000). Interactions through either component could physically connect the Gli/Cora ribbon to the F-actin prehair through spectrin; it remains to be seen, however, if the Na$^+$/K$^+$ ATPase and/or Neuroglian are apically polarized in conjunction with Gli and Cora. Previous studies in the wing in have demonstrated that actin polymerization is necessary for prehair formation and cell viability (Eaton et al., 1995; Turner and Adler, 1998). Disruption of F-actin regulation also causes wing hair phenotypes: perturbation of RhoA and its downstream effector Drok causes multiple hair phenotypes (Strutt et al., 1997; Winter et al., 2001). Application of F-actin-disrupting drugs to pupal wings also causes a multiple hair phenotype (Turner and Adler, 1998). The *Gli* hair phenotype does not include multiple hairs per cell, suggesting that prehair F-actin is correctly regulated in *Gli* mutants.

The tubulin cytoskeleton is also a potential candidate for connecting the septate junction to the apical prehair. Microtubules form a web that contacts the cell periphery at the level of Cora staining at 30 h APF (Eaton et al., 1996); additionally, microtubules are present inside the prehair after elongation (Mogensen et al., 1989). Experiments are underway to determine if the tubulin cytoskeleton is polarized to prehair bases in conjunction with Gli and Cora.

A relationship between septate junction components and the cytoskeleton may also explain the *Gli*/septate–junction marginal adhesion defects. Adhesion between wing layers is dependent on integrins at basal–basal contacts between wing layers (Brower and Jaffe, 1989; Bunch et al., 1992; Fristrom et al., 1993) and on the transalar cytoskeleton connecting them (Mogensen and Tucker, 1988; Mogensen et al., 1989). Interestingly, this dependence does not extend to the wing margin: Clones lacking β-integrin adjacent to the wing margin do not cause blisters, even when the clone spans the wing margin, placing cells lacking β-integrin into basal–basal contact (Brower and Jaffe, 1989). To our knowledge, *Gli* mutations are the first described that blister specifically at the wing margin. Adhesion in this area is thus dependent on Gli and independent of integrins. While the ultrastructure of the transalar cytoskeleton in this region has not been reported, our results suggest the possibility that the septate junction may be an alternative to integrin-based focal adhesions in this area of the wing.

Gli and Cora mediate parallel alignment independently of frizzled signaling

When a mechanism functioning to align wing hairs in parallel was first suggested, it was predicted to be *frizzled* independent (Wong and Adler, 1993). Our results have borne this prediction out. Gli and Cora are the first factors necessary for hair orientation shown to function independently of *frizzled* signaling: The localization and apical polarization of Gli and Cora does not require *fz* function; conversely, the *fz* pathway is unaffected by mutations in *Gli*. Gli and Cora are also the first factors shown to polarize in line with the distal–proximal axis in the pupal wing, the converse pattern of the *fz* pathway components. Thus, it appears that proximal-to-distal hair polarity is controlled by factors polarized in line with the anterior–posterior axis, while parallel alignment is controlled by factors polarized in line with the proximal–distal axis. Additionally, the *Gli* nonparallel phenotype appears to arise from unstable prehairs as a result of compromised, but partially functional, apically polarized Gli and Cora. The formation of the final wing hair pattern thus has two phases: the specification of the site of prehair emergence by the *fz* signaling pathway, and subsequent alignment and stabilization of extended prehairs through apically polarized septate junction components. Future experiments are necessary to determine the precise link between the apical Gli/Cora ribbon and the prehair pedestal; however, the demonstrated interactions

between F-actin/ankyrin and the septate junction markers Neuroglian and the Na$^+$/K$^+$ ATPase are likely candidates for further investigation.

References

Adler, P.N., 2002. Planar signaling and morphogenesis in *Drosophila*. Dev. Cell 2, 525–535.

Adler, P.N., Lee, H., 2001. Frizzled signaling and cell–cell interactions in planar polarity. Curr. Opin. Cell Biol. 13, 635–640.

Ashburner, M., 1989. *Drosophila*. Cold Spring Harbor Laboratory, Cold Spring Harbor, NY.

Ashburner, M., Thompson, P., Roote, J., et al., 1990. The genetics of a small autosomal region of *Drosophila* melanogaster containing the structural gene for alcohol dehydrogenase. VII. Characterization of the region around the snail and cactus loci. Genetics 126, 679–694.

Auld, V.J., Fetter, R.D., Broadie, K., et al., 1995. Gliotactin, a novel transmembrane protein on peripheral glia, is required to form the blood–nerve barrier in *Drosophila*. Cell 81, 757–767.

Axelrod, J.D., 2001. Unipolar membrane association of Dishevelled mediates Frizzled planar cell polarity signaling. Genes Dev. 15, 1182–1187.

Axelrod, J.D., 2002. Strabismus comes into focus. Nat. Cell Biol. 4, E6–E8.

Axelrod, J.D., Miller, J.R., Shulman, J.M., et al., 1998. Differential recruitment of Dishevelled provides signaling specificity in the planar cell polarity and Wingless signaling pathways. Genes Dev. 12, 2610–2622.

Bastock, R., Strutt, H., Strutt, D., 2003. Strabismus is asymmetrically localised and binds to Prickle and Dishevelled during *Drosophila* planar polarity patterning. Development 130, 3007–3014.

Basu, J., Bousbaa, H., Logarinho, E., et al., 1999. Mutations in the essential spindle checkpoint gene bub1 cause chromosome missegregation and fail to block apoptosis in *Drosophila*. J. Cell Biol. 146, 13–28.

Baumgartner, S., Littleton, J.T., Broadie, K., et al., 1996. A *Drosophila* neurexin is required for septate junction and blood–nerve barrier formation and function. Cell 87, 1059–1068.

Bennett, V., Gilligan, D.M., 1993. The spectrin-based membrane skeleton and micron-scale organization of the plasma membrane. Annu. Rev. Cell Biol. 9, 27–66.

Bhat, M.A., Izaddoost, S., Lu, Y., et al., 1999. Discs Lost, a novel multi-PDZ domain protein, establishes and maintains epithelial polarity. Cell 96, 833–845.

Bilder, D., Perrimon, N., 2000. Localization of apical epithelial determinants by the basolateral PDZ protein Scribble. Nature 403, 676–680.

Bilder, D., Schober, M., Perrimon, N., 2003. Integrated activity of PDZ protein complexes regulates epithelial polarity. Nat. Cell Biol. 5, 53–58.

Brower, D.L., Jaffe, S.M., 1989. Requirement for integrins during *Drosophila* wing development. Nature 342, 285–287.

Bunch, T.A., Salatino, R., Engelsgjerd, M.C., et al., 1992. Characterization of mutant alleles of myospheroid, the gene encoding the beta subunit of the *Drosophila* PS integrins. Genetics 132, 519–528.

Dubreuil, R.R., Maddux, P.B., Grushko, T.A., et al., 1997. Segregation of two spectrin isoforms: polarized membrane-binding sites direct polarized membrane skeleton assembly. Mol. Biol. Cell 8, 1933–1942.

Dubreuil, R.R., Wang, P., Dahl, S., et al., 2000. *Drosophila* beta spectrin functions independently of alpha spectrin to polarize the Na,K ATPase in epithelial cells. J. Cell Biol. 149, 647–656.

Eaton, S., Auvinen, P., Luo, L., et al., 1995. CDC42 and Rac1 control different actin-dependent processes in the *Drosophila* wing disc epithelium. J. Cell Biol. 131, 151–164.

Eaton, S., Wepf, R., Simons, K., 1996. Roles for Rac1 and Cdc42 in planar polarization and hair outgrowth in the wing of *Drosophila*. J. Cell Biol. 135, 1277–1289.

Einheber, S., Zanazzi, G., Ching, W., et al., 1997. The axonal membrane protein Caspr, a homologue of neurexin IV, is a component of the septate-like paranodal junctions that assemble during myelination. J. Cell Biol. 139, 1495–1506.

Fehon, R.G., Dawson, I.A., Artavanis-Tsakonas, S., 1994. A *Drosophila* homologue of membrane-skeleton protein 4.1 is associated with septate junctions and is encoded by the Coracle gene. Development 120, 545–557.

Feiguin, F., Hannus, M., Mlodzik, M., et al., 2001. The ankyrin repeat protein Diego mediates Frizzled-dependent planar polarization. Dev. Cell 1, 93–101.

Fristrom, D.K., 1982. Septate junctions in imaginal disks of *Drosophila*: a model for the redistribution of septa during cell rearrangement. J. Cell Biol. 94, 77–87.

Fristrom, D., Wilcox, M., Fristrom, J., 1993. The distribution of PS integrins, laminin A and F-actin during key stages in *Drosophila* wing development. Development 117, 509–523.

Genova, J.L., Fehon, R.G., 2003. Neuroglian, Gliotactin, and the Na+/K+ ATPase are essential for septate junction function in *Drosophila*. J. Cell Biol. 161, 979–989.

Jefford, G., Dubreuil, R.R., 2000. Receptor clustering drives polarized assembly of ankyrin. J. Biol. Chem. 275, 27726–27732.

Lamb, R.S., Ward, R.E., Schweizer, L., et al., 1998. *Drosophila* coracle, a member of the protein 4.1 superfamily, has essential structural functions in the septate junctions and developmental functions in embryonic and adult epithelial cells. Mol. Biol. Cell 9, 3505–3519.

Mogensen, M.M., Tucker, J.B., 1988. Intermicrotubular actin filaments in the transalar cytoskeletal arrays of *Drosophila*. J. Cell Sci. 91 (Pt 3), 431–438.

Mogensen, M.M., Tucker, J.B., Stebbings, H., 1989. Microtubule polarities indicate that nucleation and capture of microtubules occurs at cell surfaces in *Drosophila*. J. Cell Biol. 108, 1445–1452.

Nelson, W.J., Veshnock, P.J., 1987. Ankyrin binding to (Na+ + K+)ATPase and implications for the organization of membrane domains in polarized cells. Nature 328, 533–536.

Peifer, M., Tepass, U., 2000. Cell biology. Which way is up? Nature 403, 611–612.

Schulte, J., Tepass, U., Auld, V.J., 2003. Gliotactin, a novel marker of tricellular junctions, is necessary for septate junction development in *Drosophila*. J. Cell Biol. 161, 991–1000.

Songyang, Z., Fanning, A.S., Fu, C., et al., 1997. Recognition of unique *carboxyl*-terminal motifs by distinct PDZ domains. Science 275, 73–77.

Strutt, D.I., 2001. Asymmetric localization of frizzled and the establishment of cell polarity in the *Drosophila* wing. Mol. Cell 7, 367–375.

Strutt, D.I., 2002. The asymmetric subcellular localisation of components of the planar polarity pathway. Semin. Cell Dev. Biol. 13, 225–231.

Strutt, D.I., Weber, U., Mlodzik, M., 1997. The role of RhoA in tissue polarity and Frizzled signalling. Nature 387, 292–295.

Taylor, J., Abramova, N., Charlton, J., et al., 1998. Van Gogh: a new *Drosophila* tissue polarity gene. Genetics 150, 199–210.

Tepass, U., Tanentzapf, G., Ward, R., et al., 2001. Epithelial cell polarity and cell junctions in *Drosophila*. Annu. Rev. Genet. 35, 747–784.

Tree, D.R., Shulman, J.M., Rousset, R., et al., 2002. Prickle mediates feedback amplification to generate asymmetric planar cell polarity signaling. Cell 109, 371–381.

Turner, C.M., Adler, P.N., 1998. Distinct roles for the actin and microtubule cytoskeletons in the morphogenesis of epidermal hairs during wing development in *Drosophila*. Mech. Dev. 70, 181–192.

Usui, T., Shima, Y., Shimada, Y., et al., 1999. Flamingo, a seven-pass transmembrane cadherin, regulates planar cell polarity under the control of Frizzled. Cell 98, 585–595.

Winter, C.G., Wang, B., Ballew, A., et al., 2001. *Drosophila* Rho-associated kinase (Drok) links Frizzled-mediated planar cell polarity signaling to the actin cytoskeleton. Cell 105, 81–91.

Wolff, T., Rubin, G.M., 1998. Strabismus, a novel gene that regulates tissue polarity and cell fate decisions in *Drosophila*. Development 125, 1149–1159.

Wong, L.L., Adler, P.N., 1993. Tissue polarity genes of *Drosophila* regulate the subcellular location for prehair initiation in pupal wing cells. J. Cell Biol. 123, 209–221.

Woods, D.F., Bryant, P.J., 1991. The discs-large tumor suppressor gene of *Drosophila* encodes a guanylate kinase homolog localized at septate junctions. Cell 66, 451–464.

Woods, D.F., Hough, C., Peel, D., et al., 1996. Dlg protein is required for junction structure, cell polarity, and proliferation control in *Drosophila* epithelia. J. Cell Biol. 134, 1469–1482.

Xu, T., Rubin, G.M., 1993. Analysis of genetic mosaics in developing and adult *Drosophila* tissues. Development 117, 1223–1237.